



ARTICLE



Early Detection of Thermoacoustic Instabilities Using Hidden Markov Models

Sudeepta Mondal^a, Najah F. Ghalyan^a, Asok Ray^{a,b}, and Achintya Mukhopadhyay^c

^aDepartment of Mechanical Engineering, The Pennsylvania State University, University Park, PA, USA;

^bDepartment of Mathematics, The Pennsylvania State University, University Park, PA, USA; ^cDepartment of Mechanical Engineering, Jadavpur University, Kolkata, India

ABSTRACT

This paper presents a dynamic data-driven method for early detection of thermoacoustic instabilities in combustors based on short-length time series of sensor data, where the objective is near-real-time monitoring and active control of pressure oscillations. The main idea is to use the available data at different regimes of the combustion process to train respective hidden-variable models using the concept of Hidden Markov Modeling (HMM) as a statistical learning tool; here, (short-length) time-series data of pressure oscillations are used to infer a Markov chain with unobserved (hidden) states. The proposed HMM-based method has been validated on experimental data collected from an electrically heated Rijke tube apparatus for predicting onset of thermoacoustic instabilities. The results have been compared with those of the current state-of-the-art measurement techniques for instability growth rate and associated computational complexity. The applicability of the proposed method has been demonstrated with respect to anomaly detection and regime identification with limited data requirements, making it a potential candidate for monitoring and active control of thermoacoustic instabilities in commercial-scale combustors.

ARTICLE HISTORY

Received 9 June 2018

Revised 11 September 2018

Accepted 11 September 2018

KEYWORDS

Thermoacoustic instability; hidden Markov modeling; real-time monitoring; active control

Introduction

Thermoacoustic instabilities (TAI) in combustion systems are related to spontaneous excitation of one or more natural acoustic modes (Lieuwen and Yang, 2005). These phenomena are typically manifested by large-amplitude self-sustained pressure oscillations in the combustion chamber, which result from a feedback loop established between the heat release rate from the flame and the combustion chamber acoustics (Matveev, 2003). A major detrimental effect of TAI is resonance, which may occur if the frequency of pressure oscillations matches the natural frequency of the combustor chamber; in that case, sustained high-amplitude pressure and temperature oscillations would cause severe mechanical stresses in the structural components of the combustor, leading to thermomechanical fatigue damage and premature structural failures.

Another detrimental effect of TAI is generation of externally audible tones at intolerable levels. Hence, mitigation of TAI is a critical issue from the perspectives of both design and operation of combustion systems.

One of the major reasons for application of active TAI control techniques is their potential for adaptability to various operational regimes of the combustion process, without compromising the weight requirements of an aircraft engine. A necessary precondition for such near-real-time active control is early detection of forthcoming TAI by making use of the available sensor time-series data. This detection problem would require system identification (e.g., accurate estimation of the degree of instability) from the sensor data at fast time scales for near-real-time decision and control. The rationale is that the time scales of TAI are in milliseconds, which mandates the requirement of system identification with short data and low computational complexity of the underlying algorithms (Mukherjee and Ray, 2014; Rajagopalan and Ray, 2006; Ray, 2004; Sarkar et al., 2016) for monitoring and active control.

From the perspectives of dynamical systems, the phenomena of TAI occur due to nonlinear triggering by Hopf bifurcations. In this respect, it is a well-known practice to characterize stable/unstable operational regimes in terms of the distance from the Hopf bifurcation point by using system growth/damping rates. In this context, positive growth rate of an acoustic mode implies that it is unstable with its fluctuation amplitude growing exponentially with time. On the other hand, an acoustic mode with a negative growth rate has perturbations decaying with time (Laera et al., 2014). The growth rate information can be used directly to quantify the distance of the current operating point from the point of TAI onset. An efficient method for online monitoring of the stability margin is crucial for the decision-maker (e.g., an automated system or a human operator) to make informed decisions about changing the operating conditions, based on the existing prior knowledge of the stability map with respect to the system parameters. Such methods are passive in the sense that they should not require external stimulation to be applied on the combustion systems (Lieuwen, 2005). Several researchers have addressed this issue by developing methods of calculating the linear growth/damping rates based on sensor data of the acoustic signature of the combustion process (e.g., Hummel et al., 2017; Noiray and Denisov, 2017; Rigas et al., 2016; Li et al., 2016; Lieuwen, 2005; Yi and Gutmark, 2008).

To the best of the authors' knowledge, most of the above methods are only suitable for offline data-intensive computations, where the execution time of the underlying algorithms and their data requirements could cause large delays relative to the time scale of TAI, if applied for online condition monitoring and active control of combustion systems. Li et al. (2016) have chosen the total acoustic energy per unit cross-sectional area as a measure to characterize the transient growth. They have used physics-based modeling by modal analysis involving Galerkin decomposition. Although similar practices involving modal analysis are widely reported in literature, specifically with respect to Rijke tubes, it might be difficult to develop a model involving the complications of a wide range of parameters in an actual combustion system. Furthermore, the nonlinear and non-normal properties of such system models add to fragility (i.e., lack of robustness) of their dynamical behavior, which imply that a stable system may become unstable with a slight change in initial conditions and certain critical system parameters. Therefore, in practice, it would become difficult to specify and maintain initial conditions and critical parameters with respect to those in the modal analyses, which will complicate the calibration of these models. From these perspectives, dynamic data-driven techniques of growth rate extraction can be very useful, as they have limited dependency on the accuracy of physics-based models. Often the root mean square of the pressure signal (P_{rms}) is used as a simple measure to set a threshold for identifying the system instability. It is noted that P_{rms} also

refers to the square root of the average energy in the signal, which is closely related to the total acoustic energy approach used by Li et al. (2016). However, since the threshold may vary from one application to another, and if this concept is used for identification of operational regimes, it might be difficult to specify thresholds for different regimes with a wide range of signal-to-noise-ratio (SNR) in the sensor data. Moreover, P_{rms} -based thresholds are mostly reliable only if the data are sufficiently long in order to satisfy the requirements of statistical stationarity (Mondal et al., 2017), which deems them unsuitable to be used as a unified framework for online TAI detection and regime identification.

Other techniques of growth rate measurement have been reported in the literature, which are based on system identification from acoustic data. For example, Noiray and Denisov (2017), Boujo et al. (2016), and Noiray and Schuermans (2012, 2013) have approximated the growth dynamics of the dominant unstable mode with stochastic differential equations (SDE) governing the amplitude and phase of a randomly forced Van der Pol oscillator, driven by additive noise. Subsequently, analytical stationary solutions to the Fokker-Plank equation associated with the SDEs have been used to describe the stationary probability distribution of the acoustic signal envelope, which involves coefficients to be fitted from the acoustic data to determine the growth rate of the oscillations. However, its applicability is expected to be limited for real-time applications, where estimation of the stationary probability distributions of the acoustic envelope would most likely be subject to a significant data requirement. In practice, it might be difficult to correlate the model parameters of a Van der Pol oscillator with those of a general combustion system in terms of their physical significance.

The technical approach of Lieuwen (2005) is somewhat different, where the extent of departure of the combustion system from its stability boundary is characterized by a decrease in the effective damping rate (ζ) of the system toward zero. The strategy is based on estimating the damping rate by performing least-squares minimization procedure to determine the best fit exponential curve $\exp(-\omega\zeta t)$ for an acoustic mode with frequency ω . Lieuwen (2005) has pointed out the limitation of this method with respect to the dependence of the estimation procedure of ζ upon the time delays of the autocorrelation function, and hence the length of the time series used for the estimation. The work by Hummel et al. (2017) and Stadlmair et al. (2017) is suited in a similar framework of estimating the damping rates through curve-fitting on the autocorrelation function derived from high frequency screech-level pressure oscillations at operating conditions, where the time-scale of variations in the amplitude and phase of the unstable mode are much slower relative to the oscillatory time scale. While the method of Lieuwen (2005) was based on the damping rate estimation in the time domain, Yi and Gutmark (2008) based their work of computing damping ratios of the acoustic modes in the frequency domain, starting with a similar model for the modal dynamics of the pressure oscillations as used by Lieuwen (2005). The damping ratios were determined by fitting a smooth curve on the frequency spectrum in the vicinity of the resonant frequency peaks using a weighted least-mean-square algorithm, by utilizing a sample length of 10,000 with a sampling frequency of 5 kHz. Such frequency-domain analyses using Fast Fourier transform (FFT)/Discrete Fourier transform typically require considerable sample points for efficient representations of the power spectral densities. Boujo et al. (2016) and Hummel et al. (2017) have based the identification procedure of growth rates for linearly unstable

cases on analytically solvable SDEs and then fitted the analytical solutions against the measured time-domain data. These SDE-based frameworks are suitable for estimating the growth rate from the stationary acoustic data at different operating conditions (e.g., different equivalence ratios); in contrast, the method developed in the current paper can be used to obtain running estimates of the triggering of transient growths involved in bifurcations that are essentially non-stationary in nature. Also, for almost all of the research literature surveyed, the quantitative determination of the growth/decay rates of combustion is not completely data-driven in the sense that they require simplified (i.e., linearized and the assumed additive noise) physics-based mathematical models of pressure oscillations, which in turn makes it difficult to justify generalization of these models to handle the problem of TAI prediction, because the underlying process is highly nonlinear and is subjected to non-additive noise.

This paper proposes a dynamic data-driven method for early detection of TAI and identification of operational regimes by using short-length time series of sensor data, which is robust to the following properties:

- Variations in the length of the observed time series, used for instability prediction and regime identification.
- Inadequacies of the underlying combustion system model if any such model is used.

The application domain of the work by Rigas et al. (2016), who have reported a growth rate measurement technique based on linear fitting on the Hilbert envelope of the unsteady pressure time-series data, is similar to the experimental data used in the current paper. The data requirements of the proposed method have been compared with those of (Rigas et al., 2016) .

Since the focal area of the reported work is early detection of instabilities, analyses have been performed using pressure time-series data that undergo transient behavior from a stable operation to limit-cycle oscillations. Furthermore, pressure sensing is commonly used in many real-life combustion systems. Thus, implementation using pressure data readily demonstrates suitability of the proposed method for practical situations. The main idea here is to use primarily experimentally generated acoustic sensor data from different regimes of the combustion process to train relevant hidden-variable models using the concept of hidden Markov modeling (HMM) (Rabiner, 1989) that has been widely used as a statistical learning tool for analysis of uncertain dynamical systems; in these applications, the associated temporal data are used to infer a Markov chain with unobserved states. For example, Menon et al. (2003) and Chen et al. (2011) have used the HMM concept for online predictive monitoring and fault detection in gas turbine engines. The trained HMM contains the latent information of the system's dynamical characteristics at different regimes of operation. In the testing phase, with a window of observation sequence (e.g., pressure time series), it is possible to find the likelihoods of the observed data sequence with respect to the pre-trained HMM. With a sliding-window calculation of the model likelihoods, an appropriate norm based on likelihood ratio has been chosen as the metric for detecting instabilities, which shows a monotonically increasing trend as the time-series signals approach limit cycle behavior through the transient mode of operation. This trend is consistent with the increasing fluctuation amplitudes of the signal during the transients,

and thus can be directly correlated to the overall growth rate of pressure oscillations (Hummel et al., 2017). It is also noted that data-driven methods, which have been studied for classification of unstable and stable modes in combustion systems, have largely focused on the usage of (statistically weak-sense stationary) stable or unstable time-series data (Gotoda et al., 2012; Nair and Sujith, 2014; Sarkar et al., 2016). The proposed method, in addition, is capable of handling non-stationary data such that the embedded information can be gainfully used for system identification. The results derived from experimental data have shown that it is possible to achieve good accuracy of detection even with a short window of time series (e.g., data over window sizes of about 10 ms corresponding to a sampling frequency of 8192 Hz), which matches with the time scale of TAI evolution. Such detection techniques are relevant for real-time monitoring and active control of TAI, where fast and computationally efficient detection/classification can provide appropriate lead-time to the actuators. From these perspectives, the major contributions of this paper are delineated below:

- (a) Development of data-driven, HMM-based robust algorithms to facilitate near-real-time monitoring and active control of thermoacoustic instabilities from short-length time series of pressure oscillations.
- (b) Experimental validation of the above algorithms on an electrically heated Rijke tube apparatus.

The laboratory apparatus and experimental procedure

The experimental data to validate the proposed concept have been generated from a laboratory-scale electrically heated Rijke tube apparatus as shown in Figure 1. It is well known that Rijke tubes possess some of the important characteristics of practical combustion systems like gas turbine combustors (for example, acoustically compact localized heat source). The simplicity of the experimentation and their capability of generating clean signals have made electrically heated Rijke tubes popular for investigations on fundamental aspects of thermoacoustic instabilities and their control (Gelbert et al., 2012). The apparatus comprises a 1.50 m long horizontal Rijke tube with an external cross-section of 0.1 m \times 0.1 m and a wall thickness of approximately 6.35 mm. The inlet air flow is supplied by a compressor, which is prone to pressure fluctuations and is also expected to have moisture and other impurities. A Parker P32E series air filter-regulator is used to suppress the pressure fluctuations and to filter the impurities. The mean air flow is then controlled through a 0–1000 standard liters per minute (LPM) Alicat mass flow controller. The heating element in the Rijke tube is a square weave 40 \times 40 nichrome wire mesh which is brazed to two copper strips on a machinable ceramic frame (Matveev, 2003) and is placed at about quarter length of the tube from the air input end (i.e., $x/L = 0.25$). The heating element is powered by a TDK Lambda programmable (0–8 V DC, 0–400 Amps) DC power source (Gopalakrishnan and Sujith, 2014). The horizontal arrangement of the tube allows an independent control of the flow rate and the heater power. Two damping chambers are provided at the two ends of the tube in order to ensure that the tube ends are maintained at pressure nodes under open-open boundary conditions. The damping

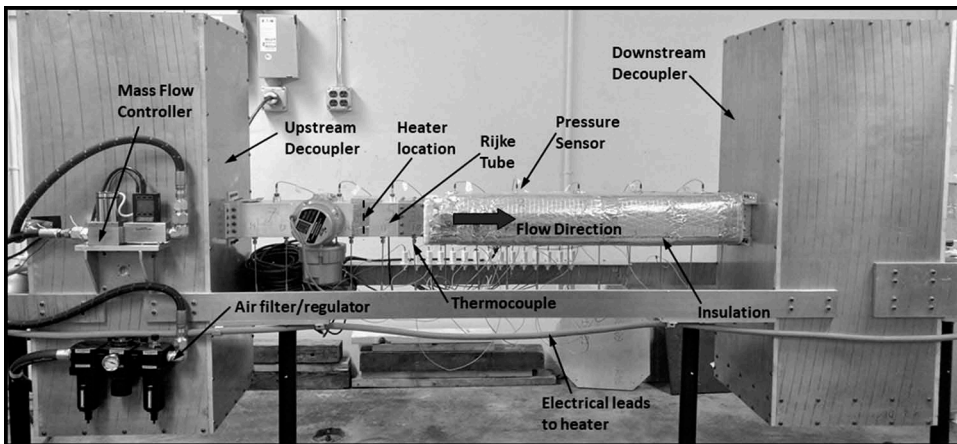


Figure 1. The Rijke tube experimental apparatus.

chambers also serve in decoupling the acoustics of the tube from those of the main air line. The chamber dimensions are $0.45 \text{ m} \times 0.45 \text{ m} \times 1.14 \text{ m}$. As a safety measure against the downstream half of the tube is insulated to reduce heat loss and to guard against any accidental physical contact with the hot metal surface.

Eight PCB-116B03 pressure sensors and fifteen K-type Omega thermocouple probes have been used for acquiring the acoustic and temperature data from the experiments. The first and the eighth pressure sensors are placed at a distance of 125 mm from the tube ends, while the distance between two consecutive sensors is approximately 180 mm. The sensors are powered through an 8-channel unity gain signal conditioner. The pressure sensors have a high sensitivity of 6 pC/psi and are coupled with in-line charge converters having an amplification of 100 mV/pC. The 13 out of the 15 thermocouple probes are placed downstream of the heater with an intermediate spacing of 90 mm, while the remaining two are placed upstream starting with a distance of approximately 63 mm from the upstream tube end. The thermocouple probes are capable of measurements up to 1360°C . All sensors are flush-mounted with the inner walls of the Rijke tube to reduce friction in air flow path. The sensor data acquisition and the voltage input to the programmable power supply unit are automated using DAQ devices from National Instruments (NI) in conjunction with NI LabVIEW 2016. The pressure sensor data is acquired through an NI-9205 (C Series Voltage Input Module) and the thermocouple data through an NI-9213 (C Series Temperature Input Module). The DC voltage supply is controlled through an NI-9264 (C Series Voltage Output Module).

The pressure sensor data are sampled at a rate of 8192 Hz and the acquired data are filtered with a 20th order Butterworth high-pass filter having a cutoff frequency of 40 Hz in order to eliminate low-frequency noises and acoustics from the damping chambers along with other environmental effects. To find the stability map of the system, steady state runs are performed after the tube is subjected to a warming up phase. After each experiment, a cool-off settling period is maintained to ensure similar steady-state initial temperature fields in the tube for each experiment. Maintaining similar initial temperatures ensure that the mean velocity of the sound waves in the air

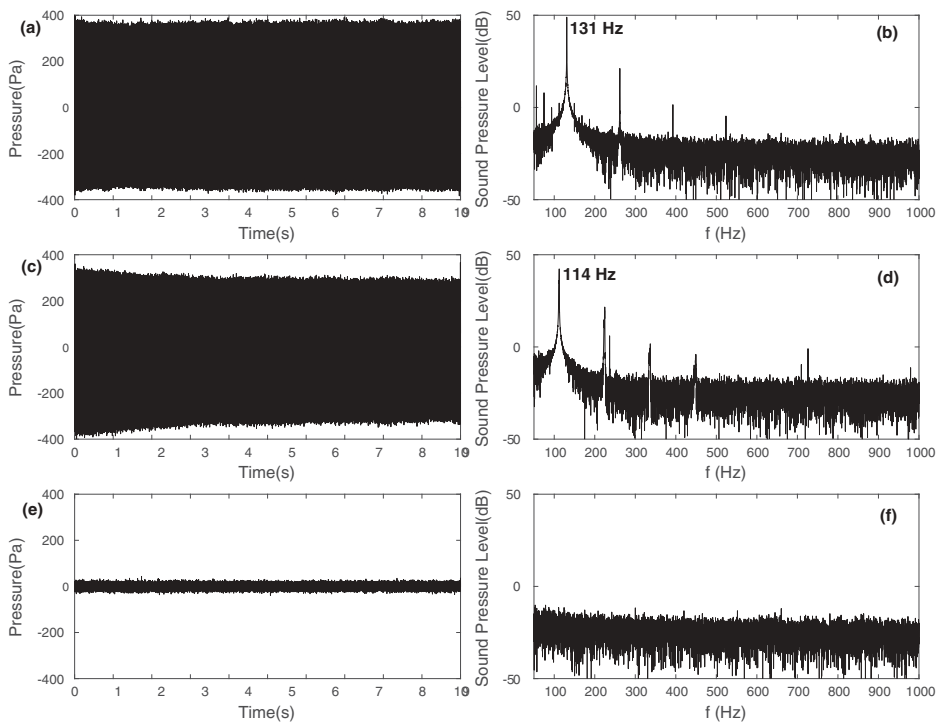


Figure 3. Representative plots of fluctuating pressure amplitudes (left) and their respective power spectral densities (right) at different operating conditions. (a) and (b): $E_{in} = 1400$ W, $Q = 162$ LPM. (c) and (d): $E_{in} = 600$ W, $Q = 112$ LPM. (e) and (f): $E_{in} = 1400$ W, $Q = 228$ LPM.

Mathematical background: hidden Markov modeling

This section briefly introduces the essential concepts of HMM, which form the building block for analyzing combustion dynamics as presented in this paper. Further details are available in Rabiner (1989), Murphy (2012), Bishop (2007), and Hajek (2015).

The concept of HMM has been widely used for representation of long-range dependencies between observations, where the underlying models are assumed to be probabilistic functions of the hidden states (Murphy, 2012). Considering a discrete-time representation of a sequence $\mathbf{Y} = \{y_1, y_2, \dots, y_T\}$ of T continuous (i.e., real-valued) observations, and assuming a first-order Markov property (Bishop, 2007) over the observations, the joint probability density function of \mathbf{Y} is obtained as:

$$p(\mathbf{Y}) = p(y_1) \prod_{t=1}^{T-1} p(y_{t+1}|y_t) \quad (1)$$

Although the above assumption has been widely used in practice, it may not be valid in many applications because of long-range correlations among the observations (Bishop, 2007; Murphy, 2012).

The HMM belongs to a class of doubly embedded stochastic processes, with a latent stochastic process of *hidden* state evolution. Although this evolution is not directly observed, it can be inferred by observing another stochastic process that produces the

sequence of observations (Rabiner and Juang, 1993), which captures the long-range dependencies among observations and enables the usage of HMMs as black-box density models on observation sequences. The major difference between the HMM and the standard Markov model is that the HMM does not assume the Markov property (i.e., conditionally dependence on the states and being independent of each other) for the observations themselves. Instead, the hidden state sequence $Z = \{z_1, z_2, \dots, z_T\}$ are assumed to follow Markovian dynamics, i.e., given the current state z_t , the future state z_{t+1} is independent of all the states prior to time instant t . Figure 4 illustrates the idea with a Bayesian network model of a simple HMM. Following the convention of directed graphical models in the left hand plate of Figure 4, a shaded node z_i denotes a hidden variable, an unshaded (i.e., clear) node y_i denotes an observed variable and an arrow denotes conditional dependence. In the right hand plate of Figure 4, the arrows denote the transitions from state Z_i to Z_j with probability a_{ij} , where the states belong to a finite and discrete set \mathcal{Q} and the cardinality $|\mathcal{Q}| = K$ is a positive integer.

To formalize the mathematical structure, let a string of observations $\{y_1, \dots, y_T\}$ be assumed to be generated by a hidden state sequence $\{z_1, \dots, z_T\}$. An HMM is then constructed as a triplet $\lambda = \{A, B, \pi\}$ (Rabiner, 1989), where:

(a) $A \triangleq [a_{ij}]$ is the $K \times K$ state-transition probability matrix:

$$a_{ij} = p(z_{t+1} = q_j | z_t = q_i) : q_i, q_j \in \mathcal{Q}$$

where $\sum_j a_{ij} = 1 \forall i$.

(b) $B \triangleq [b_j(y_t)]$ is the probability density of the observation given the state:

$$b_j(y_t) = p(y_t | z_t = q_j)$$

(c) $\pi \triangleq [\pi_i]$ is the probability distribution of the initial state z_1 : $\pi_i = p(z_1 = q_i)$, where π is a $1 \times K$ vector with $\sum \pi_i = 1$.

Following the above model λ , the corresponding joint probability distribution of states and observations has the form:

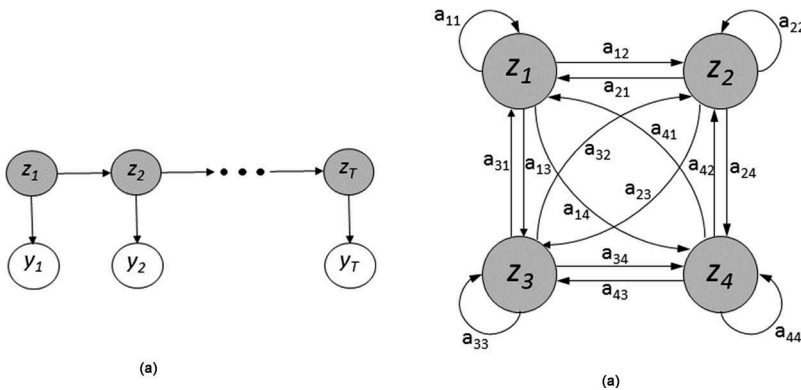


Figure 4. Left hand plate: Bayesian network model of an HMM showing conditional dependence of observations with hidden Markov states. Right hand plate: state transitions in a 4-state HMM (i.e., $K = 4$).

$$p(\mathbf{Y}, \mathbf{Z}) = p(z_{1:T})p(y_{1:T}|z_{1:T}) = \left[p(z_1) \prod_{t=1}^{T-1} p(z_{t+1}|z_t) \right] \left[\prod_{t=1}^T p(y_t|z_t) \right] \quad (2)$$

Here the HMM is assumed to have a continuous real-valued observation model, where the observations $\{y_1, \dots, y_T\}$ are one-dimensional and their emission probability follows a Gaussian mixture model:

$$p(y_t|z_t = q_j, \lambda) = \sum_{\ell=1}^M c_{j\ell} \mathcal{N}(y_t, \mu_{j\ell}, \Sigma_{j\ell}) \quad (3)$$

where $\sum_{\ell=1}^M c_{j\ell} = 1, \forall j \in \{1, \dots, K\}$; M is the number of Gaussian mixture components; and $\mathcal{N}(y_t, \mu_{j\ell}, \Sigma_{j\ell})$ represents Gaussian density function of y_t with mean $\mu_{j\ell}$ and covariance $\Sigma_{j\ell}$ associated with state q_j and mixture component ℓ .

Two main model parameters are, therefore, the number of hidden states (K) and the number of mixture components (M), which need to be optimally selected in the context of HMMs (Celeux and Durand, 2008; Rydén, 1995); and AIC/BIC based techniques (Akaike, 1974; Schwarz, 1978) are most commonly used to select the optimal model parameters that maximize the likelihood of the data and minimize the model complexity, thereby balancing the goodness of fit against model complexity to alleviate data overfitting. This paper has adopted the BIC model selection function for choosing the parameters K and M . Thus, the model learning problem is to find the optimal set of parameters for $\lambda = \{A, B, \pi\}$ in order to maximize $P(\mathbf{Y}|\lambda)$. It is achieved through a commonly used iterative procedure called *Baum-Welch Algorithm* which is an application of Expectation-Maximization method for inferring HMM parameters (Rabiner, 1989).

Now, given an observation sequence $\mathbf{Y} = \{y_1, y_2, \dots, y_T\}$ and an HMM model λ , the problem at hand is to find the probability of the entire observation sequence so that it can be associated with the most likely model from a bank of pre-trained HMM models. This is expressed as:

$$p(\mathbf{Y}|\lambda) = \sum_{\mathbf{Z}} p(\mathbf{Y}|\mathbf{Z}, \lambda)p(\mathbf{Z}|\lambda) = \sum_{z_1, z_2, \dots, z_T} \pi_{z_1} b_{z_1}(y_1) a_{z_1 z_2} b_{z_2}(y_2) \dots a_{z_{T-1} z_T} b_{z_T}(y_T) \quad (4)$$

The calculation of $p(\mathbf{Y}|\lambda)$ according to the direct definition as in Eq. (4) has computational complexity in the order of $(2TK^T)$ which may become intractable for even small values of K and T . For numerical efficiency, the well-known *Forward Procedure* is used, which reduces computational complexity to the order of (K^2T) . The relevant algorithms are briefly discussed in the following subsections.

A. The forward procedure

The forward variable $\alpha_t(i)$, defined as $\alpha_t(i) \triangleq p(y_1, y_2, \dots, y_t, z_t = q_i|\lambda)$ is the probability that, provided the model λ is being followed, the partial observation sequence $\{y_1, y_2, \dots, y_t\}, 1 \leq t < T$ until time t ends with the state of the system being q_i at time t . This can be solved inductively as follows:

$$1. \text{ Initialization step : } \alpha_1(i) = \pi_i b_i(y_1), \quad 1 \leq i \leq K \quad (5)$$

$$2. \text{ Induction step : } \alpha_{t+1}(j) = \left[\sum_{i=1}^K \alpha_t(i) a_{ij} \right] b_j(y_{t+1}), \quad 1 \leq t \leq T-1, \quad 1 \leq j \leq K \quad (6)$$

$$3. \text{ Termination step : } p(\mathbf{Y}|\lambda) = \sum_{i=1}^K \alpha_T(i) \quad (7)$$

where the parameters T and K are the same as defined earlier.

B. The backward procedure

The backward variable $\beta_t(i)$, defined as $\beta_t(i) \triangleq p(y_{t+1}, y_{t+2}, \dots, y_T | z_t = q_i, \lambda)$, is the probability of the partial observation sequence $\{y_{t+1}, y_{t+2}, \dots, y_T\}$ from $t+1$ till the end, provided that the state at time t is q_i and the model followed is λ . This can be solved inductively as follows:

$$1. \text{ Initialization step : } \beta_T(i) = 1, \quad 1 \leq i \leq K \quad (8)$$

$$2. \text{ Induction step : } \beta_t(i) = \left[\sum_{j=1}^K a_{ij} b_j(y_{t+1}) \beta_{t+1}(j) \right], \quad t = T-1, T-2, \dots, 1, \quad (9)$$

$$1 \leq i \leq K$$

where the parameters T and K are the same as defined earlier.

C. Model learning: Baum-Welch algorithm

The model learning problem requires the estimation of the model parameters $\lambda = \{A, B, \pi\}$ so as to maximize the likelihood $p(\mathbf{Y}|\lambda)$. Baum-Welch algorithm is a recursive estimation procedure of the HMM parameters. Given the model and the observation sequence, the intermediate variables ξ and γ are defined, for $1 \leq i \leq K$, $1 \leq j \leq K$ and $1 \leq t \leq T$, as:

$$\xi_t(i, j) \triangleq P(z_t = q_i, z_{t+1} = q_j | \mathbf{Y}, \lambda) \quad (10)$$

$$\gamma_t(i) \triangleq p(z_t = q_i | \mathbf{Y}, \lambda) \quad (11)$$

The variables γ_t and $\xi_t(i, j)$ are expressed in terms of the forward and backward variables α_t and β_t , defined earlier as:

$$\gamma_t(i) = \frac{\alpha_t(i) \beta_t(i)}{p(\mathbf{Y}|\lambda)} = \frac{\alpha_t(i) \beta_t(i)}{\sum_{i=1}^K \alpha_t(i) \beta_t(i)}, \quad (12)$$

$$\xi_t(i, j) = \frac{\alpha_t(i) a_{ij} b_j(y_{t+1}) \beta_{t+1}(j)}{\sum_{i=1}^K \sum_{j=1}^K \alpha_t(i) a_{ij} b_j(y_{t+1}) \beta_{t+1}(j)}$$

Using the above relations, and the fact that $y_t(i) = \sum_{j=1}^K \xi_t(i, j)$, it is possible to estimate $\{A, B, \pi\}$ as:

$$\hat{\pi}_i = \gamma_1(i) \quad (13)$$

$$\hat{a}_{ij} = \frac{\sum_{t=1}^{T-1} \xi_t(i, j)}{\sum_{t=1}^{T-1} \gamma_t(i)} \quad (14)$$

$$\hat{c}_{jk} = \frac{\sum_{t=1}^T \tilde{\gamma}_t(j, k)}{\sum_{t=1}^T \sum_{k=1}^M \tilde{\gamma}_t(j, k)} \quad (15)$$

$$\hat{\mu}_{jk} = \frac{\sum_{t=1}^T \tilde{\gamma}_t(j, k) \cdot y_t}{\sum_{t=1}^T \tilde{\gamma}_t(j, k)} \quad (16)$$

$$\hat{\Sigma}_{jk} = \frac{\sum_{t=1}^T \tilde{\gamma}_t(j, k) \cdot (y_t - \mu_{jk})^2}{\sum_{t=1}^T \tilde{\gamma}_t(j, k)} \quad (17)$$

where $\tilde{\gamma}_t(j, k)$ is the probability of being in state q_j at time t with the k^{th} mixture component. That is,

$$\tilde{\gamma}_t(j, k) = \left[\frac{\alpha_t(j)\beta_t(j)}{\sum_{j=1}^N \alpha_t(j)\beta_t(j)} \right] \left[\frac{c_{jk}\mathcal{N}(y_t, \mu_{jk}, \Sigma_{jk})}{\sum_{k=1}^M c_{jk}\mathcal{N}(y_t, \mu_{jk}, \Sigma_{jk})} \right] \quad (18)$$

It is noted that the term $\tilde{\gamma}_t(j, k)$ generalizes to $\gamma_t(j)$ in case of a single-component Gaussian density (i.e., $M = 1$) or a (discrete) probability mass function.

The model $\hat{\lambda} = \{\hat{A}, \hat{B}, \hat{\pi}\}$ can be recursively estimated until it converges to a local maxima of the likelihood function $p(\mathbf{Y}|\lambda^*)$, where λ^* is the maximum likelihood estimate of the HMM. More details on the Baum-Welch algorithm and forward-backward algorithm are available in (Hajek, 2015; Rabiner, 1989).

Technical approach

This section presents the technical approach for autonomous detection of thermoacoustic instabilities (TAI) based on time series of pressure oscillations, where regime identification is an important and challenging task. In this context, Rigas et al. (2016) have demonstrated on a Rijke tube apparatus, similar to the apparatus described earlier, that a transition can be made from a stable fixed point to a limit-cycle mode of operation if the heater power is increased beyond the Hopf bifurcation point (Thompson and Stewart, 1986). Since thermoacoustic instabilities are understood to be an outcome of subcritical Hopf bifurcations, it is imperative to devise efficient detection methodologies that can identify the shift in operational regime during an early transient period, before it reaches a limit-cycle behavior. This is the rationale for having a rich source of data that will be capable of demonstrating the transient behavior of the pressure time series as the combustion system passes through the bifurcation point. The following procedure, similar to the one demonstrated by Rigas et al. (2016), has been adopted in this paper:

- The experimental apparatus is heated to a steady state with the primary heater power input (E_{in}) ≈ 200 W.
- Then, the power input is abruptly increased to a higher value that showed limit cycle behavior as depicted in the stability chart in Figure 2.
- For each experiment, the air flow rate (Q) has been set at a constant value, and a series of experiments have been conducted with Q ranging from 130 LPM to 250 LPM at increments of 20 LPM.
- Pressure data have been recorded using the acoustic sensors over a 30-s window at a sampling rate of 8192 Hz.

During each experiment, within the aforesaid 30-s window, the transition data from the stable regime to an unstable (limit-cycle) regime (which occurs through the bifurcation point) have been collected from the pressure sensors. The ensemble of collected data contains unsteady pressure signals for several experimental conditions having respective responses with different amplitudes of limit-cycle oscillations. This dataset provides a rich source of information for the three regimes, namely, stable, transient, and unstable (limit-cycle), which is used for learning generative statistical models of these three operational regimes. It is noted that the SNR may vary with individual sensors, as seen in the typical profiles of pressure signals in Figure 5. For the data profile of a pressure sensor (immediately downstream of the heater) in Figure 5(a), the power input is abruptly increased to 1800 W at time ~ 17 s from the initial 200 W preheated condition and the air flow rate is kept constant at 210 LPM; Figure 5(b) shows qualitatively similar responses from another pressure sensor (further downstream of the heater), where the power input has been abruptly increased to 2000 W at time ~ 17 s from the initial 200 W preheated condition and the air flow rate is kept constant at 250 LPM. The SNR in the data collected from these two sensors is also different due to their proximities from the heater, as seen in the textures of the time series in Figure 5(a) as compared to those in Figure 5(b).

Having the domain knowledge of stable, transient and the limit-cycle operational regimes, the task at hand is to train three HMMs: λ_i , for $i \in \{1, 2, 3\}$, where λ_1 corresponds to the stable regime of operation, λ_2 corresponds to the transient growth regime, and λ_3 corresponds to the unstable (limit-cycle) regime. This task accomplishes a generative modeling of the system dynamics based on the domain knowledge procured by the

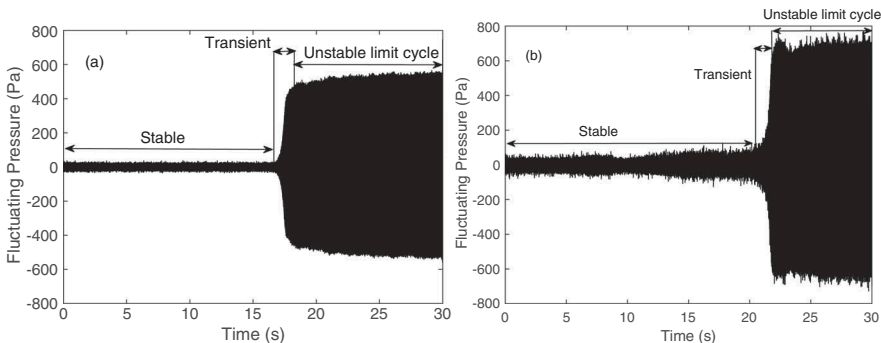


Figure 5. Unsteady pressure signals showing the transience from stable fixed point to limit cycle through bifurcation. (a) E_{in} abruptly increased to 1800 W with $Q = 210$ LPM. (b) E_{in} abruptly increased to 2000 W keeping $Q = 250$ LPM.

experiments. It is noted that although the experiments have been conducted to encompass a wide range of operating conditions and power input profiles to the heating unit, it is infeasible to conduct experiments under all different operational conditions that a real-life combustor may undergo. Nevertheless, the HMMs are intended to learn the trend in the data that are used for training the models. So, with a sufficiently rich set of training data procured from different regimes, HMMs can be used to encapsulate the dynamics of the behavioral characteristics of the combustion system in different regimes. Such a “context-based” learning makes sense in this respect because, for example, the signature of the pressure signals in the unstable (limit-cycle) regime is expected to have a deterministic periodic nature, which is much different from the noisy or chaotic nature generally exhibited in the stable regime. Learning generative models based on ensembles of data from these three operational regimes ensures that the underlying model is robust to uncertainties such as variations in operational conditions and sensor noise even for a single operational regime.

Test data of pressure time series have been used with the pre-trained models for early detection of thermoacoustic instabilities (TAI). Given a window of time series $\{y_1, \dots, y_T\}$, the log-likelihood L_k and the log-likelihood ratio (LLR) $[L_k - L_1]$ are obtained as:

$$\begin{aligned} (L_k \stackrel{\Delta}{=} \log p(y_{1:T})|\lambda_k) \text{ for } k = 1, 2, 3) \\ \Rightarrow ([L_k - L_1] = \log \left[\frac{(p(y_{1:T})|\lambda_k)}{(p(y_{1:T})|\lambda_1)} \right] \text{ for } k = 2, 3) \end{aligned} \quad (19)$$

where $(p(y_{1:T})|\lambda_k)$ denotes the probability that the observed pressure time series is generated by the HMM λ_k , for $k \in \{1, 2, 3\}$. The rationale here is that as the system deviates from the stable regime and the transient growth tends toward limit-cycle instabilities, the signature of pressure oscillations would have a higher probability to be generated from either λ_2 or λ_3 than from λ_1 , which is reflected from the LLR $[L_k - L_1]$ in Eq. (19) being positive for $k = 2, 3$.

Focusing on short-length windows of time series in this paper to address real-time monitoring and active control, early detection of TAI would provide appropriate lead-time for the actuators to implement the control action. The procedure involved in the analysis is described as follows:

- (a) The window size is chosen for a time scale of ~10–100 ms, because the bifurcation mode of instability evolution occurs in the time scale of milliseconds. Hence, online detection of TAI with such a length of time window should be able to provide appropriate lead-time to the actuators to implement the control actions for suppressing the pressure oscillation.
- (b) Time-series data in subsequent batches of the chosen window length is used to calculate $(p(y_{1:T})|\lambda_k)$, for $k = 1, 2$ and 3.
- (c) The LLR in Eq. (19) is chosen as the norm for detecting instability onset. The ratio is calculated for each batch of data being analyzed and condition monitoring is performed based on the evolution of the norm over batches of time-series samples.

Results and discussions

This section presents the results of experimental validation of the proposed HMM-based method on the Rijke tube apparatus and compares these results with the results of similar data-driven techniques on the same data sets for estimating the growth rates of thermo-acoustically unstable systems.

A. Detection of early onset of instabilities

This subsection presents the results for detecting instabilities during the transient regime. The dataset used for this purpose comprises an ensemble of 145 sets of pressure time series with 30-s duration similar to those depicted in Figure 5. This entire dataset has been randomly divided into training and testing sets in the ratio 80:20. The training data are first used to train the three HMMs, λ_1 , λ_2 and λ_3 . The test data for detection of TAI are chosen to be truncated just before the onset of unstable (limit-cycle) regime, and the performance of the classifier for instability detection is based on successful detection of the onset of short-duration transients even before the limit cycle begins. This requirement poses a stringent condition on the classifier to perform early detection of instability evolution with dynamic sensor data. The idea here is that the underlying algorithm should be able to detect a divergence from the stable regime (i.e., nominal operation) well within the transient regime sufficiently before the unstable (limit-cycle) regime begins; this is necessary because a major failure can be triggered by structural resonance in the unstable regime when it might be too late to exercise control actions. The testing phase involves calculating the LLR in Eq. (19)) for classifying each data window. In the framework of Bayesian binary hypothesis testing, the proposed algorithm classifies each pressure time-series window into either *stable* (Class A) or *unstable* (Class B) based on the following LLR test (see also Eq. (19)):

$$[L_k - L_1] = \log \left[\frac{(p(y_{1:T})|\lambda_k)}{(p(y_{1:T})|\lambda_1)} \right] = \log[(p(y_{1:T})|\lambda_k)] - \log[(p(y_{1:T})|\lambda_1)] \stackrel{H}{\underset{G}{\gtrless}} \tau \text{ for } k = 2 \text{ or } 3 \quad (20)$$

where τ is a user-specified threshold (Poor, 2013). A commonly used criterion to choose τ is the receiver operating characteristic (ROC) curve that is obtained by varying τ to provide a trade-off between the probability of successful detection ($p_D \triangleq p[\text{Decided Class} = H | \text{True Class} = H]$) and the probability of false alarms ($p_F \triangleq p[\text{Decided Class} = H | \text{True Class} = G]$).

Figure 6 shows a family of ROC curves for the proposed HMM-based detection algorithm using different window sizes of data, with the likelihood ratio chosen as $\log \left[\frac{(p(y_{1:T})|\lambda_2)}{(p(y_{1:T})|\lambda_1)} \right]$ (i.e., the probability that each observed sequence belongs to the transient class as compared with the probability of belonging to the stable class), abbreviated as $[L_2 - L_1]$ henceforth. Similar ROC curves are obtained when the likelihood is compared with respect to the unstable and stable classes, i.e., $\log \left[\frac{(p(y_{1:T})|\lambda_3)}{(p(y_{1:T})|\lambda_1)} \right]$ (abbreviated as $[L_3 - L_1]$) is used as the LLR. Due to the fact that data textures in the transient and unstable (limit-cycle) regimes are significantly different from those in the stable regime, LLRs generated

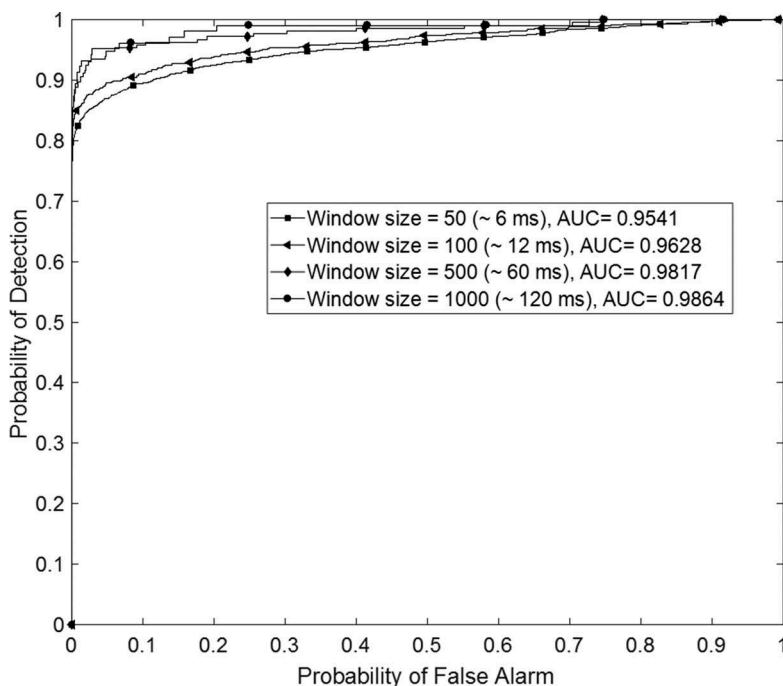


Figure 6. ROC curves for the proposed method with different window sizes of sensor time series.

by these two methods may be largely similar. Therefore, either $[L_2 - L_1]$ or $[L_3 - L_1]$ can be used as the classifier.

Window sizes of 50, 100, 500 and 1000 have been chosen for the plots in Figure 6, which corresponds to time scales in the order of milliseconds considering the sampling frequency of 8192 Hz. For example, a window size of 50 corresponds to a classifier decision taken after approximately every 6 ms. A commonly used method for comparing the performance of different classifiers is comparison of the area under the curve (AUC) of ROC for each classifier (Fawcett, 2006). Higher AUC is generally associated with a better overall performance of a classifier. As depicted in Figure 6, the AUC increases from 0.9541 to 0.9864 as the window size is increased from 50 to 1000, with progressively higher detection rates at specified false alarm rates. The rationale is that the classifier is expected to perform better with respect to larger lengths of observation sequences. It is worth reiterating that the anomalous class detected by the classifier in Figure 6 belongs to the transient phase of pressure time series, and hence, the high classification accuracy even with approximately 6–60 ms long data makes the proposed HMM-based classification scheme a promising candidate for TAI detection in an early part of the transient regime.

The trend in the variations of the LLR is now investigated as the time series passes through the transient regime. For demonstration purposes, the pressure signature recorded by the downstream sensor nearest to the heater has been chosen for the

experimental condition of increasing the heater power input abruptly to 2000 W while maintaining the flow rate at 250 LPM (see Figure 5(b)).

The testing data are analyzed according to batches of a chosen window length of 100 samples. Since the objective is early detection of TAI, the batches are continually analyzed for the entire time series until the limit-cycle instability is reached. Figure 7 shows the evolution of the LLR $[L_2 - L_1]$ (plotted with squares on solid line) as the sensor data are analyzed in batches of data length 100. The pressure time-series data are plotted by downsampling the actual time-series data by 100, because each successive log-likelihood calculation involves 100 pressure observation data. The vertical dashed line in Figure 7 indicates the separation between the stable and transient regimes. The onset of instabilities occurs after about 1700th sample, which corresponds to ~ 20 s in the actual time scale. It is noted that the associated LLR also changes abruptly from approximately zero value before the 1700th time sample to a very high positive value in the order of $\sim 10^4$, showing a very high sensitivity to the divergence of the pressure profile characteristics from the stable regime to the transient regime. In addition, the monotonicity in the increase of LLR is correlated to the degree of instability of pressure oscillations, which justifies its potential use as an index for measure of instabilities. This shows that the pre-trained HMMs are able to promptly distinguish the onset of transient growth from the stable regime early in the transient regime. The high sensitivity of the proposed detection method is attributed to the non-deterministic algebraic structure of HMMs along with its trained observation emission distribution, which results in a very good discriminative performance even with short lengths of observation.

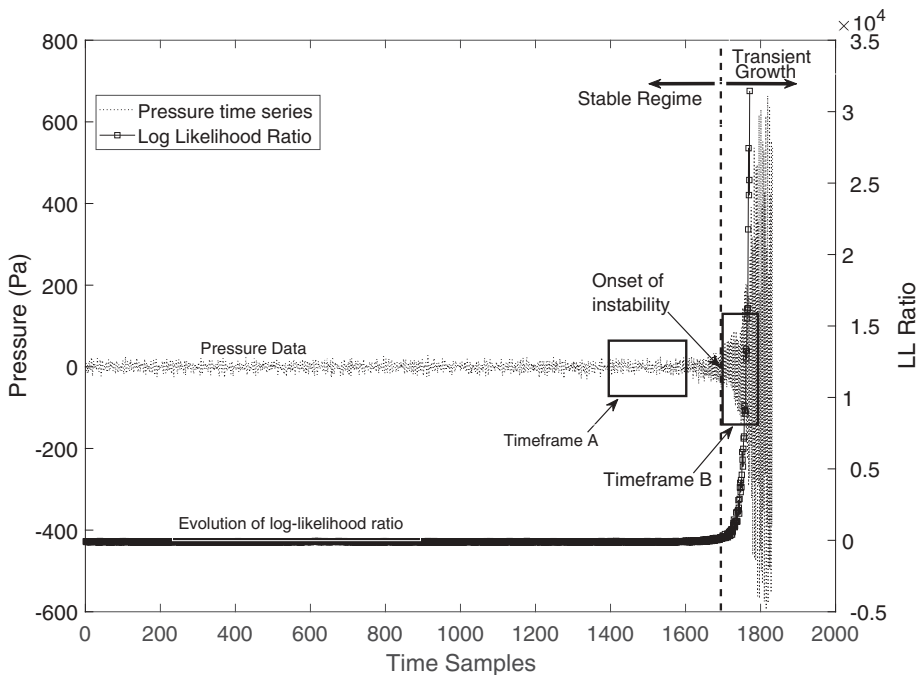


Figure 7. Evolution of LLR $[L_2 - L_1]$ (see Eq. (19)) with the pressure time-series data.

B. Regime detection

More insight is obtained from Figure 7 by analyzing the variations of the likelihoods with respect to λ_1, λ_2 and λ_3 in Timeframe A (1400–1600 samples) in the stable regime and Timeframe B (1600–1800 samples) in an early part of the transient regime. This is reflected in Figure 8 from the highest relative likelihood L_1 of the data corresponding to λ_1 (downfacing solid triangles), as compared with likelihoods L_2 and L_3 with respect to λ_2 (solid squares) and λ_3 (hollow circles), respectively. λ_3 has the lowest likelihood among the three, which can be traced back to the fact that λ_3 has been trained with data belonging to the unstable (limit-cycle) regime, the deterministic and periodic nature of which is quite different from the chaotic nature of stable regime data.

Figure 9 shows the evolution of the three likelihoods in Timeframe B of Figure 7 which spans from 1600 to 1800 time samples – the region of early transience from stable to unstable behavior. It is seen that the likelihood of the data belonging to the stable model λ_1 sharply drops as soon as the transience sets in, and this results in the sharp increase in the value of the LLR $[L_2 - L_1]$ as depicted in Figure 7. The respective variations in L_2 and L_3 are conspicuously observed in the inset of Figure 9. It is seen that L_2 dominates L_3 for the bulk of the Timeframe B, except at the very end when limit cycle behavior sets in, which causes L_3 to dominate L_2 . Although both L_3 and L_2 should be able to distinguish the occurrence of anomalous behavior from L_1 , the LLR $[L_2 - L_1]$ is expected to be more discriminative than the LLR $[L_3 - L_1]$ for transient regime detection.

From the perspective of regime classification, the HMMs exhibit a potential to discriminate between the transient and unstable (limit-cycle) data with respect to the pressure time-series signals. Figure 10 shows the evolution of L_2 and L_3 as the time series

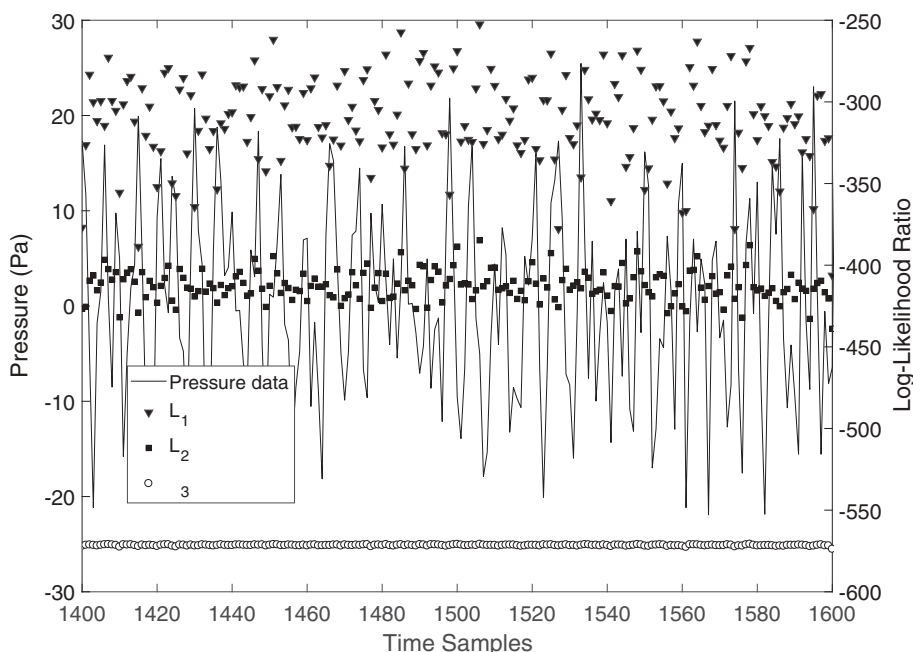


Figure 8. Log-likelihoods L_1, L_2 and L_3 (see Eq. (19)) with pressure samples in Timeframe A of Figure 7.

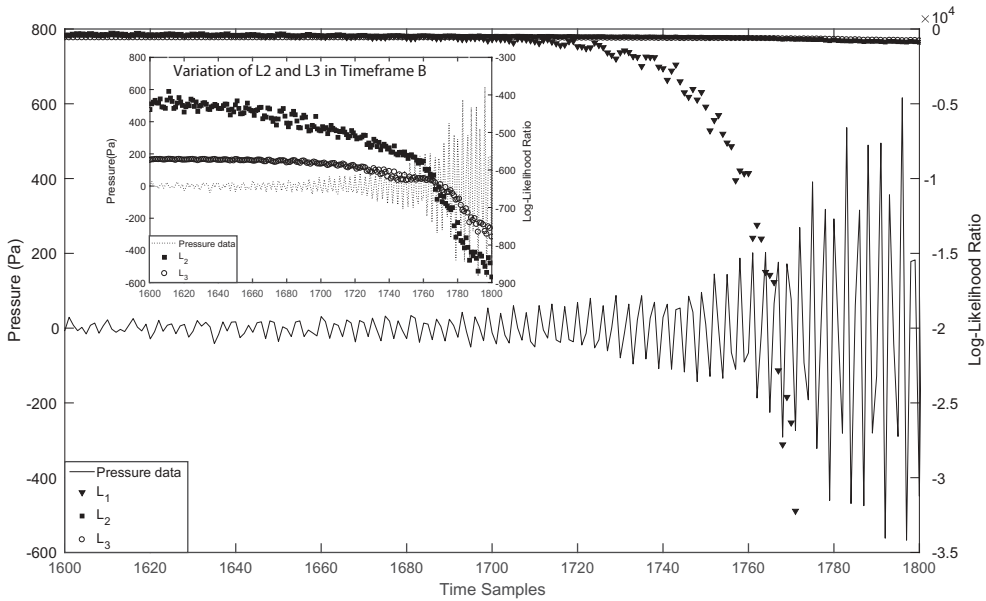


Figure 9. Log-likelihoods L_1 , L_2 and L_3 (see Eq. (19)) with pressure samples in Timeframe B of Figure 7. The inset shows explicitly the variations of the log-likelihoods L_2 and L_3 within this timeframe.

passes from transient to unstable (limit-cycle) regime. It is seen that L_3 starts dominating L_2 as the unstable (limit-cycle) regime is approached, showing that the models have satisfactorily captured the dynamics of the system during the different regimes. So, for regime detection purposes, the information from the ROC curves (Figure 6) can be used to choose a particular threshold τ corresponding to the trade-off between the detection rate required by the user and the allowable false alarm in detection. The problem of regime detection is challenging because the classifier has to decide which of the three pre-trained regimes does a short data history belong to. Table 1 presents the regime detection accuracies, where the threshold τ has been chosen using the ROC of a classifier with $[L_3 - L_1]$ as the LLR with window size = 100; here τ has been chosen to correspond to about 92% detection rate with 10% allowable false alarm from the ROC curve.

The test data samples consist of 1000 random samples from each of the three regimes, which were classified using the chosen threshold of $[L_3 - L_1]$. The limit cycle unstable regime was distinguished from the transient growth regime by employing the LLR $[L_3 - L_2]$. It is interesting to note that the classifier designed for detecting instabilities in the transient regime is able to detect the unstable (limit-cycle) regime with 100% accuracy, implying that the detection algorithm is almost always sure to distinguish limit cycle data from the other two regimes. The superior performance in detecting unstable (limit-cycle) data is possibly due to its deterministic periodic nature. However, the presence of transience in the data makes its detection even more difficult and the method discussed in this paper can serve as a unified framework for this purpose.

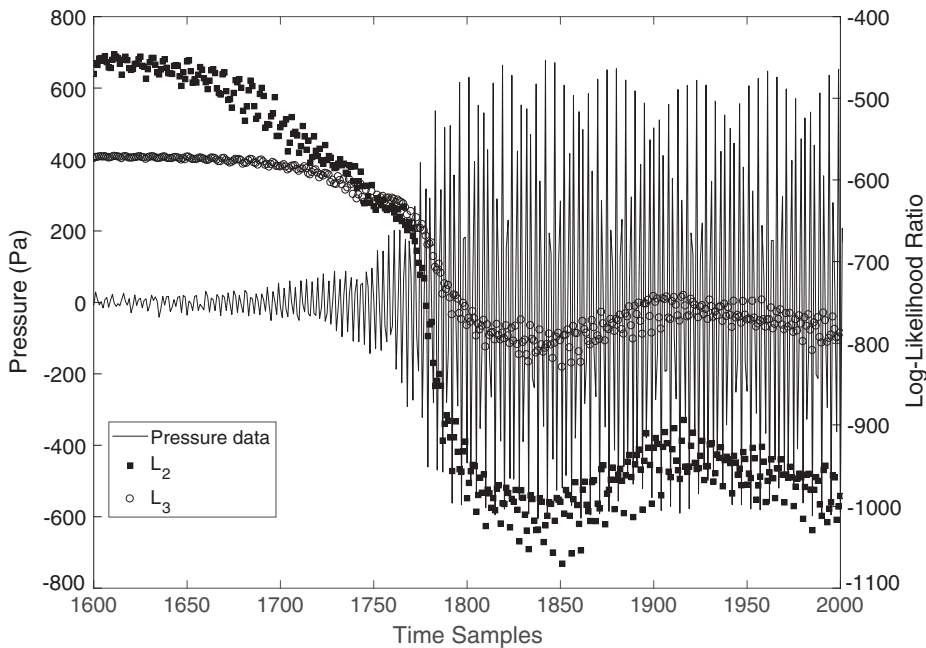


Figure 10. Log-likelihoods L_2 and L_3 (see Eq. (19)) with samples from transient to limit cycle regimes.

Table 1. Classification accuracy of the three regimes.

Stable regime	Transient regime	Unstable regime
90%	91%	100%

C. Comparison with growth rate measurement techniques

Information about the growth rates of linearly unstable systems has been shown to be useful for the design of robust controllers (Noiray and Schuermans, 2012). In fact, for real-time monitoring and active control of thermoacoustic instabilities, the growth rate information can be used to detect the onset of unstable modes. However, it is difficult to characterize the growth rate from an experimental point of view, as discussed by Moeck et al. (2007). An unstable combustion system generally exhibits an abrupt change from a stable regime to an unstable (limit-cycle) regime through a bifurcation, thereby posing serious challenges for data-driven growth rate extraction techniques to detect the growing trend in the data in that short period. Recently, Rigas et al. (2016) and Jamieson et al. (2017) have reported growth and decay rate measurements using transient acoustic time-series data from an electrically heated Rijke tube, similar to the apparatus used in the current paper. Their method is based on extracting clean regions of linear growth and decay from the Hilbert envelope of the time-series signal, and measuring the growth rate by a linear fit in the identified region. The application of this method to the current data is first reported and then certain issues are discussed related to the data length requirements.

The extraction of growth rate is based on the assumption that the combustion dynamics are governed by a single thermoacoustic mode, which is the dominant frequency of the self-excited oscillations (Lieuwen, 2003). Under this single mode approximation, the calculated growth rate

is essentially that of the dominant mode (ω) of the system (Boujo et al., 2016), which is around 130 Hz for the data analyzed in this section. To implement this concept, the time-series data from the Rijke tube apparatus have been filtered using a 20th order bandpass Butterworth IIR filter with lower 3-dB frequency of 120 Hz and higher 3-dB frequency of 140 Hz, in conjunction with a phase equalizing filter for preventing phase distortion in the filtered signal. This helps in reducing the noise and extracting clean regions of linear growth, which can then be identified by thresholding on the Hilbert amplitude to separate the approximately linear region between the noise floor and the nonlinearly dominated regions.

Figure 11 shows the evolution of the Hilbert envelope as a function of data length for the case when the heater power was increased abruptly to 1400 W with the air flow rate kept constant at 170 LPM. It can be seen in Figure 11(b) that it is possible to define upper and lower thresholds on the Hilbert amplitude to formulate a linear fit for extracting the linear growth rate as $\sigma_r = \frac{d(\log(\text{Amplitude}))}{dt}$ when the Hilbert transform is performed on the complete data, as reported by Rigas et al. (2016). In Figure 11(c) the time-series data have been truncated to choose 1000 samples from the 18.5-s mark around which the system starts exhibiting transient growth. Since this sample window contains data from the transient regime, it should be associated with a positive linear growth rate of the dominant mode.

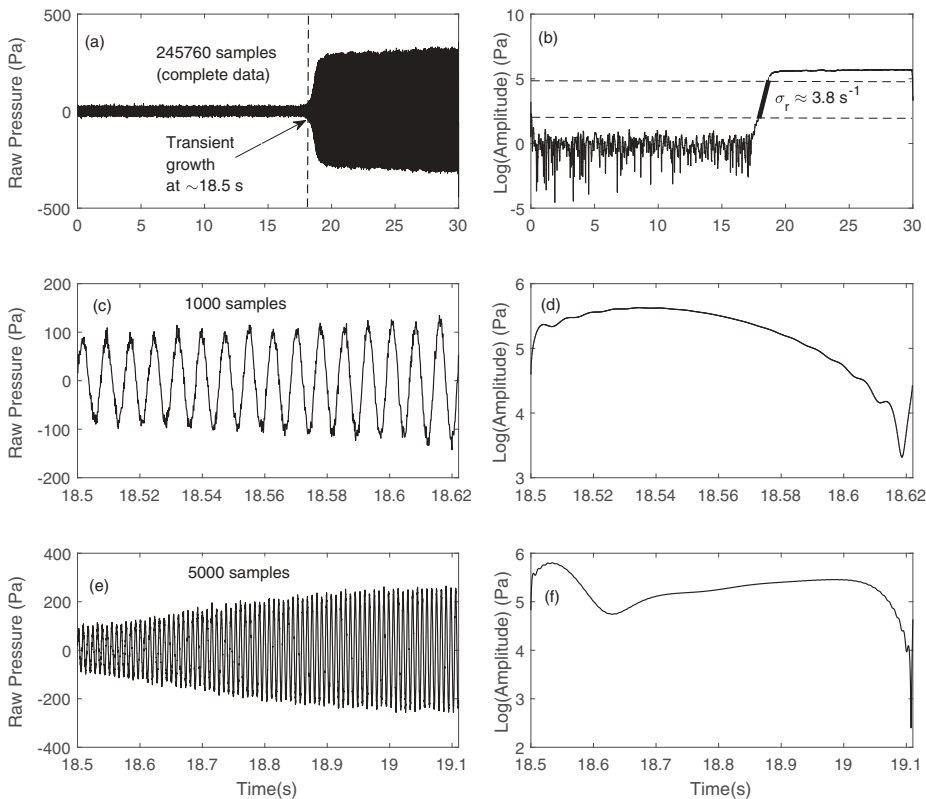


Figure 11. Hilbert envelope calculated from the pressure time-series data. (a), (c) and (e): Complete pressure data from 0 to 30 s (245,760 samples), from 18.5 to 18.62 s (1000 samples), from 18.5 to 19.1 s (5000 samples), respectively. (b), (d) and (f): Evolution of Hilbert envelope for cases (a), (c) and (e), respectively. The linear fit for calculating growth rate is shown as a bold line in (b).

The Hilbert envelope evolution in Figure 11(d) does not involve a similar linearly growing region from which the growth rate can be extracted. This is possibly because the envelope evolves slowly, and hence it requires more data. As seen in Figure 11(f), even when the data length was increased to 5000 samples from the 18.5-s mark, the Hilbert envelope does not show a conspicuous region of growth that can be described by a linear fit. Hence, although this technique can be used as an offline method to calculate the growth rate for different operating conditions, it is limited in its applicability as an online detection tool for extracting the growth rate of a dynamically evolving unstable thermoacoustic system. Moreover, the amplitude thresholds for the regions of noise floor and nonlinearity are expected to vary across different time samples, and would most likely be a strong function of the operating conditions and varying SNR of the sensors from which the samples are generated.

With the LLRs of the HMMs, one may classify short-length time windows in the transient regime, as was discussed earlier. For the time series with 1000 samples in Figure 11(c), $[L_2 - L_1] = 1.4303 \times 10^4$ (see Eq. (19)), and for the one with 5000 samples (Figure 11(e)), $[L_2 - L_1] = 44.814 \times 10^4$. Both the values are well above 0, implying that the data samples are far from the stable regime. If a sample size of 1000 can be afforded, a windowed likelihood calculation can be performed to find the trend in variation of the likelihood ratio, which would reflect the rate of growth in the time sample. Figure 12 shows the comparison between LLR variations using 1000 samples and the growth rate calculation using the complete dataset. Two cases have been investigated, Case 1 in which the power input has been increased to 1400 W keeping the flow rate constant at 170 LPM, and Case 2 in which the power input has been increased to 2000 W with the flow rate kept fixed at 230 LPM. Figure 12(a) shows the growth rates calculated using the complete time series of 30 s, with solid line representing Case 1 and dotted line representing Case 2 that has a higher growth rate of 4.4 s^{-1} as compared to 3.8 s^{-1} in Case 1. This is reflected in the likelihood ratio plot in Figure 12(b), where $[L_2 - L_1]$ has been calculated using a window size of 100 samples on a time-series sample of 1000 data points chosen from the inception of transient growth in both the cases. Case 2 (dotted line with triangles) in Figure 12(b) shows a progressively increasing rate of higher relative likelihood of λ_2 with respect to λ_1 , which is consistent with the information obtained from the growth rate calculations. Since the likelihood ratio can be used to conclude the higher rate of growth using a much shorter time series from the early transient period, it can potentially be applicable to early detection of the rate of transient growth in the unstable regime.

D. Comparison of computational complexity with other data-driven techniques

To the best of the authors' knowledge, the current paper is the first reported work that aims to detect the growth of instabilities from non-stationary time-series data using a real-time data-driven approach. Most of the research reported in the combustion literature have proposed different data-driven tools for predicting precursors to instabilities from stationary time-series data, for example, steady-state pressure time series obtained as a function of equivalence ratio. Sarkar et al. (2016) have reported computational complexity of different data-driven methods for prediction of thermoacoustic instabilities using stationary time-series data. Nair and Sujith (2014) have correlated loss of multifractality with the onset of instability in the acoustic fluctuations by computing generalized Hurst exponents. Gotoda et al. (2012) have studied variations in the minimum of normalized permutation entropy as a function of equivalence

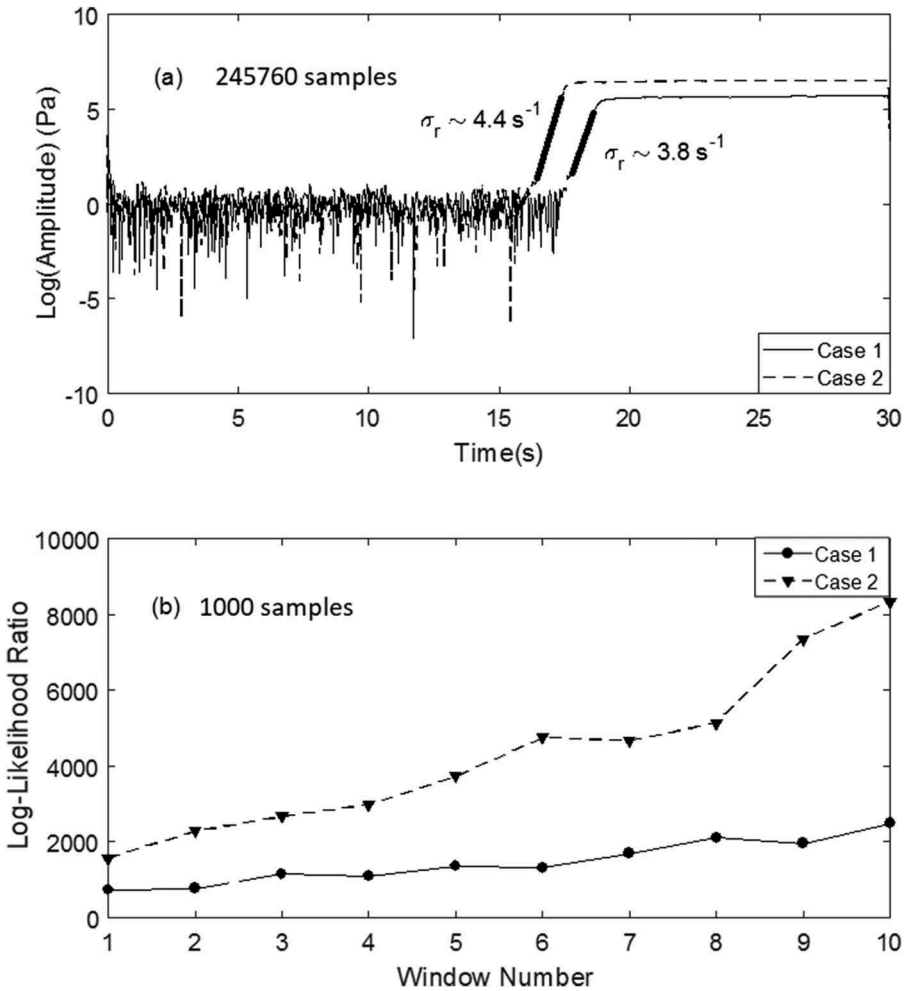


Figure 12. Comparison of growth rates with log-likelihood evolution. (a) Growth rate calculation using Hilbert envelope. (b) Variation of LLR [$L_2 - L_1$] (see Eq. (19)) in an early growth period of the two cases.

ratio to measure the degree of complexity in the dynamic nature of the acoustic fluctuations with the onset of instability. Sarkar et al. (2016) proposed a data-driven technique of monitoring the state complexity of D -Markov machines which starts dropping as the combustion system tends to become unstable. This is consistent with the observations (Gotoda et al., 2012) with regard to variations in the complexity of the pressure data. Sarkar et al. (2016) also proposed a method of detecting instabilities by appropriately thresholding on the variation of the $\times D$ -Markov entropy rates from heterogeneous sensors, namely, pressure and chemiluminescence data.

These methods have been applied for predictions of instability with respect to steady state response at different operating conditions, and they are, in a way, different from the method proposed in this paper which attempts to detect the growth of instabilities as a result of bifurcation resulting in the triggering of transient growth to limit cycles. However, it is still worth comparing the computational complexity of all these methods because they can be posed as potential competitors in their

applications to predicting the degree of instability in the steady state response of the combustion system. For example, with respect to the Rijke tube apparatus described in this paper, the steady state response of the system after a set point of power input is reached can be recorded and studied with two HMMs corresponding to stable and unstable modes of operation. With this domain knowledge incorporated in the training phase, LLR-based methods can be used to calculate the relative likelihoods of the steady state acoustic signature as a function of power inputs to study the degree of instability in the acoustic behavior. Table 2 compares the average online processing times of the techniques mentioned above with the time complexity of the LLR [$L_2 - L_1$] calculation. The comparison is carried out in the MATLAB-2014 environment on a computation platform of Dell Precision T3400 PC with Intel(R) Core(TM) 2 Quad CPU Q9550 @ 2.83GHz and 2.83 GHz. As discussed earlier, the calculation of the likelihood $p(\mathbf{Y}|\lambda)$ using *Forward Algorithm* has a complexity of $\sim |Q|^2 T$. This is reflected in the almost linear increment of the processing time with respect to the data length for calculating the likelihood ratio [$L_2 - L_1$] (dashed line with circles). The likelihood ratio computation time fares better than that of the minimum permutation entropy method, although the time complexities for the computation of both the Hurst Exponent and $\times D$ -Markov entropy rate are lesser. However, it is worth mentioning here that HMMs are a class of more complex non-deterministic models representing the probabilistic behavior of temporal data and it can be used directly to solve the problem of regime detection with relatively short-length data, for which direct applicability of other methods have not been reported. Moreover, the HMM framework, in principle, can be trained with other classes of instabilities like lean blowout or screech with data generated from simulations/experiments, and hence can be extended for detection of various undesirable regimes of operation, subject to sufficient training experience. Also, the focal area of this paper is to portray the applicability of the HMM-LLR method for data lengths less than 1000 samples (~ 120 ms, with sampling frequency, $F_s = 8192$ Hz). Such short data lengths have not been used previously in the other aforementioned techniques for instability detection in stationary data. Table 3 lists the processing times for the online calculation of LLR using the different window lengths as described in Figure 6. Hence, the competitive time complexity of the HMM LLR along with its performance robustness even at very short data lengths makes it a

Table 2. Time complexity of different methods for detection of combustion instabilities.

Data length (s)	Processing times of different data-driven methods (s)			
	Hurst exponent	$\times D$ -Markov entropy rate	Minimum permutation entropy	Log-likelihood ratio
0.2	0.019	0.056	0.095	0.035
0.4	0.025	0.059	0.135	0.068
0.6	0.031	0.062	0.174	0.011
0.8	0.035	0.065	0.213	0.132
1.0	0.041	0.068	0.252	0.164

Table 3. Time complexity of LLR calculation in the online phase.

Number of samples ($F_s = 8192$ Hz)	50	100	500	1000
Data length (ms)	6	12	60	120
Processing time (ms)	4	6	12	23

potentially suitable method for regime detection and instability classification, which is a key element for real-time detection and active control of combustion instabilities.

Summary, conclusions, and future work

This paper has developed and validated a non-deterministic statistical modeling tool for early detection of thermoacoustic instabilities and identification of operational regimes in combustion systems. The analysis is based on learning HMM to represent the typical behavior of the combustion system with data from different regimes, and using the models for predicting the most likely regime from a short test sequence of acoustic pressure recordings. This method focuses on real-time applications with short windows of pressure time series without compromising the accuracy of prediction of thermoacoustic instabilities and identification of the associated operational regimes. The proposed HMM-based method has been validated on experimental data from an electrically heated Rijke tube apparatus for predicting the onset of thermoacoustic instabilities. The results of the proposed method have been compared with those of similar data-driven techniques on the same data sets for estimating growth rates of thermoacoustically unstable systems (e.g., linear fitting from Hilbert envelope of the pressure time series). The proposed HMM-based method yielded consistent observations on the growth rate detection, albeit requiring significantly lower data history for its efficient implementation and applicability. While the proposed method is found to be robust with respect to spurious process and measurement noise, the response of the detection algorithm is sensitive to small changes in the regime characteristics, which makes it very suitable for detection of texture changes in the temporal signature of the acoustic data.

The proposed method is suitable for real-time anomaly detection and regime identification based on short-length time series of pressure oscillations. Since real-time active control of thermoacoustic instabilities (TAI) is a problem of major concern in the development of reliable combustion systems, the technique presented in this paper can serve as a computationally efficient tool for real-time detection of operational regimes from online measurements with parsimonious data requirements, making it a potentially effective for real-time active control of TAI.

While there are many areas of theoretical and experimental research to enhance the work reported in this paper, the authors suggest the following topics for future research:

- (a) Development of a unified detection framework addressing other modes of instabilities (e.g., lean blowouts).
- (b) Extension of the proposed HMM-based method for detection of instabilities in combustion systems operating under different kinds of protocols.
- (c) Extension of the probabilistic approach in the reported work to state estimation for forecasting of future states for prediction of the temporal behavior.
- (d) Implementation of the HMM-based method for (closed-loop) active control of the laboratory-scale apparatus with actuators for controlling instabilities.
- (e) Enhancement of computational efficiency of the HMM-based method further by using variational inference-based learning of the probabilistic models (Murphy, 2012).

Pertinent acronyms

AUC	Area under the curve
DFT	Discrete Fourier transform
HMM	Hidden Markov modeling
LLR	Log-likelihood ratio
LPM	Liters per minute
ROC	Receiver operating characteristic
SNR	Signal to noise ratio
SDE	Stochastic differential equation
TAI	Thermoacoustic instabilities

Disclaimer

Any opinions, findings and conclusions or recommendations expressed in this publication are those of the authors and do not necessarily reflect the views of the sponsoring agencies.

Funding

The work reported in this paper has been supported in part by the U.S. Air Force Office of Scientific Research (AFOSR) under Grant Nos. FA9550-15-1-0400 and FA9550-18-1-0135 in the area of dynamic data-driven application systems (DDDAS).

References

- Akaike, H. 1974. A new look at the statistical model identification. *IEEE Trans. Autom. Control*, **19** (6), 716–723. doi:10.1109/TAC.1974.1100705.
- Bishop, C. 2007. *Pattern Recognition and Machine Learning*. Springer, New York, NY.
- Boujo, E., Denisov, A., Schuermans, B., and Noiray, N. 2016. Quantifying acoustic damping using flame chemiluminescence. *J. Fluid Mech.*, **808**, 245–257. doi:10.1017/jfm.2016.663.
- Celeux, G., and Durand, J.-B. 2008. Selecting hidden Markov model state number with cross-validated likelihood. *Comput. Stat.*, **23**(4), 541–564. doi:10.1007/s00180-007-0097-1.
- Chen, J., Hsu, T.-Y., Chen, C.-C., and Cheng, Y.-C. 2011. Online predictive monitoring using dynamic imaging of furnaces with the combinational method of multiway principal component analysis and hidden Markov model. *Ind. Eng. Chem. Res.*, **50**(5), 2946–2958. doi:10.1021/ie100671j.
- Fawcett, T. 2006. An introduction to ROC analysis. *Pattern Recognit. Lett.*, **27**(8), 861–874. ROC Analysis in Pattern Recognition. doi:10.1016/j.patrec.2005.10.010.
- Gelbert, G., Moeck, J.P., Paschereit, C.O., and King, R. 2012. Feedback control of unstable thermoacoustic modes in an annular rijke tube. *Control Eng. Pract.*, **20**(8), 770–782. doi:10.1016/j.conengprac.2012.03.016.
- Gopalakrishnan, E.A., and Sujith, R.I. 2014. Influence of system parameters on the hysteresis characteristics of a horizontal rijke tube. *Int. J. Spray Combust. Dyn.*, **6**(3), 293–316. doi:10.1260/1756-8277.6.3.293.
- Gotoda, H., Amano, M., Miyano, T., Ikawa, T., Maki, K., and Tachibana, S. 2012. Characterization of complexities in combustion instability in a lean premixed gas-turbine model combustor. *Chaos: Interdiscip. J. Nonlinear Sci.*, **22**(4), 043128. doi:10.1063/1.4766589.
- Hajek, B. 2015. *Random Processes for Engineers*. Cambridge University Press, Cambridge, UK.
- Hummel, T., Berger, F., Stadlmair, N., Schuermans, B., and Sattelmayer, T. 2017. Extraction of linear growth and damping rates of high-frequency thermoacoustic oscillations from time domain data. *ASME Turbo Expo: Power for Land, Sea, and Air*, Vol. 4A, Combustion, Fuels and Emissions. doi:10.1115/GT2017-64233. ISBN: 978-0-7918-5084-8
- Jamieson, N.P., Rigas, G., and Juniper, M.P. 2017. Experimental sensitivity analysis via a secondary heat source in an oscillating thermoacoustic system. *Int. J. Spray Combust. Dyn.*, **9**(4), 230–240. doi:10.1177/1756827717696325.

- Laera, D., Campa, G., Camporeale, S.M., Bertolotto, E., Rizzo, S., Bonzani, F., Ferrante, A., and Saponaro, A. 2014. Modelling of thermoacoustic combustion instabilities phenomena: application to an experimental test rig. *Energy Procedia*, **45**, 1392–1401. ATI 2013–68th Conference of the Italian Thermal Machines Engineering Association. doi:10.1016/j.egypro.2014.01.146.
- Li, X., Zhao, D., Yang, X., Wen, H., Jin, X., Li, S., Zhao, H., Xie, C., and Liu, H. 2016. Transient growth of acoustical energy associated with mitigating thermoacoustic oscillations. *Appl. Energy*, **169**, 481–490. doi:10.1016/j.apenergy.2016.01.060.
- Lieuwen, T. 2005. Online combustor stability margin assessment using dynamic pressure data. *J. Eng. Gas Turbines Power*, **127**(3), 478–482. doi:10.1115/1.1850493.
- Lieuwen, T.C. 2003. Statistical characteristics of pressure oscillations in a premixed combustor. *J. Sound Vib.*, **260**(1), 3–17. doi:10.1016/S0022-460X(02)00895-7.
- Lieuwen, T.C., and Yang, V. 2005. Combustion instabilities in gas turbine engines: operational experience, fundamental mechanisms, and modeling. *Am. Inst. Aeronautics Astronautics*, **1**, 3–26. chapter Matveev, K. (2003), Thermoacoustic instabilities in the Rijke tube: experiments and modeling, PhD thesis, California Institute of Technology.
- Menon, S., Uluyol, O., Kim, K., and Nwadiogbu, E.O. (2003), Incipient fault detection and diagnosis in turbine engines using hidden Markov models.
- Moeck, J., Bothien, M., Paschereit, C., Gelbert, G., and King, R. (2007), Aerospace Sciences Meetings, American Institute of Aeronautics and Astronautics, chapter Two-Parameter Extremum Seeking for Control of Thermoacoustic Instabilities and Characterization of Linear Growth.
- Mondal, S., Bhattacharya, C., Chattopadhyay, P., Mukhopadhyay, A., and Ray, A. (2017), AIAA propulsion and energy forum, American Institute of Aeronautics and Astronautics, Chapter: Prediction of Thermoacoustic Instabilities in a Premixed Combustor based on FFT-based Dynamic Characterization.
- Mukherjee, K., and Ray, A. 2014. State splitting and merging in probabilistic finite state automata for signal representation and analysis. *Signal Process.*, **104**, 105–119. doi:10.1016/j.sigpro.2014.03.045.
- Murphy, K. 2012. *Machine Learning: A Probabilistic Perspective*, 1st ed.. Cambridge, MA, USA: The MIT Press
- Nair, V., and Sujith, R.I. 2014. Multifractality in combustion noise: predicting an impending combustion instability. *J. Fluid Mech.*, **747**, 635–655. doi:10.1017/jfm.2014.171.
- Noiray, N., and Denisov, A. 2017. A method to identify thermoacoustic growth rates in combustion chambers from dynamic pressure time series. *Proc. Combust. Inst.*, **36**(3), 3843–3850. doi:10.1016/j.proci.2016.06.092.
- Noiray, N., and Schuermans, B. 2012. Theoretical and experimental investigations on damper performance for suppression of thermoacoustic oscillations. *J. Sound Vib.*, **331**(12), 2753–2763. doi:10.1016/j.jsv.2012.02.005.
- Noiray, N., and Schuermans, B. 2013. Deterministic quantities characterizing noise driven Hopf bifurcations in gas turbine combustors. *Int. J. Non Linear Mech.*, **50**, 152–163. doi:10.1016/j.ijnonlinmec.2012.11.008.
- Poor, H.V. 2013. *An Introduction to Signal Detection and Estimation*. New York, NY, USA: Springer Science & Business Media.
- Rabiner, L., and Juang, B.-H. 1993. *Fundamentals of Speech Recognition*, Prentice-Hall, Inc., Upper Saddle River, NJ.
- Rabiner, L.R. 1989. A tutorial on hidden Markov models and selected applications in speech recognition. *Proc. IEEE*, **77**(2), 257–286. doi:10.1109/5.18626.
- Rajagopalan, V., and Ray, A. 2006. Symbolic time series analysis via wavelet-based partitioning. *Signal Process.*, **86**(11), 3309–3320. doi:10.1016/j.sigpro.2006.01.014.
- Ray, A. 2004. Symbolic dynamic analysis of complex systems for anomaly detection. *Signal Process.*, **84**(7), 1115–1130. doi:10.1016/j.sigpro.2004.03.011.
- Rigas, G., Jamieson, N.P., Li, L.K.B., and Juniper, M.P. 2016. Experimental sensitivity analysis and control of thermoacoustic systems. *J. Fluid Mech.*, **787**. doi.org/10.1017/jfm.2015.715
- Rydén, T. 1995. Estimating the order of hidden Markov models. *Statistics*, **26**(4), 345–354. doi:10.1080/02331889508802501.

- Sarkar, S., Chakravarthy, S.R., Ramanan, V., and Ray, A. 2016. Dynamic data-driven prediction of instability in a swirl-stabilized combustor. *Int. J. Spray Combust. Dyn.*, **8**(4), 235–253. doi:[10.1177/1756827716642091](https://doi.org/10.1177/1756827716642091).
- Schwarz, G. 1978. Estimating the dimension of a model. *Ann. Statist.*, **6**(2), 461–464. doi:[10.1214/aos/1176344136](https://doi.org/10.1214/aos/1176344136).
- Stadlmair, N.V., Hummel, T., and Sattelmayer, T. (2017), Thermoacoustic damping rate determination from combustion noise using bayesian statistics, *ASME Turbo Expo 2017: Turbomachinery Technical Conference and Exposition* (50848), V04AT04A025.
- Thompson, J., and Stewart, H. 1986. *Nonlinear Dynamics and Chaos*, John Wiley, Chichester, UK
- Yi, T., and Gutmark, E.J. 2008. Online prediction of the onset of combustion instability based on the computation of damping ratios. *J. Sound Vib.*, **310**(1), 442–447. doi:[10.1016/j.jsv.2007.07.072](https://doi.org/10.1016/j.jsv.2007.07.072).